

Collapse of Particle-Laden Interfaces under Compression: Buckling vs Particle Expulsion

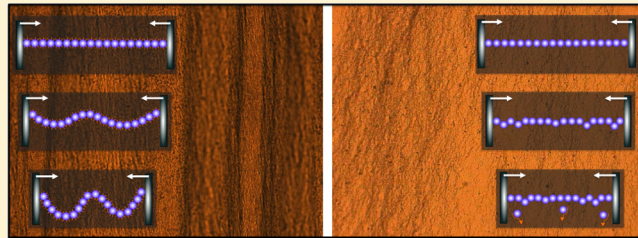
Sepideh Razavi,[†] Kathleen D. Cao,[‡] Binhua Lin,[§] Ka Yee C. Lee,[‡] Raymond S. Tu,[†] and Ilona Kretzschmar^{*,†}

[†]Department of Chemical Engineering, City College of City University of New York, New York, New York 10031, United States

[‡]Department of Chemistry, Institute for Biophysical Dynamics, and James Franck Institute and [§]James Franck Institute and Center for Advanced Radiation Sources, The University of Chicago, Chicago, Illinois 60637, United States

Supporting Information

ABSTRACT: Colloidal particles can bind to fluid interfaces with a capillary energy that is thousands of times the thermal energy. This phenomenon offers an effective route to emulsion and foam stabilization where the stability is influenced by the phase behavior of the particle-laden interface under deformation. Despite the vast interest in particle-laden interfaces, the key factors that determine the collapse of such an interface under compression have remained relatively unexplored. In this study, we illustrate the significance of the particle surface wettability and presence of electrolyte in the subphase on interparticle interactions at the interface and the resulting collapse mode. Various collapse mechanisms including buckling, particle expulsion, and multilayer formation are reported and interpreted in terms of particle–particle and particle–interface interactions.



consequential for the structure of the formed interfacial layers and their response to deformations.^{16–21}

Of particular interest is the response of silica,^{9,22–25} polystyrene,^{26–30} and metallic^{31–34} particulate layers to compression for which different collapse mechanisms have been reported. Here, we briefly summarize major findings obtained for interfaces covered with silica and polystyrene particles owing to their technological significance in emulsion and foam stabilization. In one of the earliest studies on silica glass beads (75 μm) of different surface wettabilities, particle expulsion to the bulk is reported for more hydrophilic samples, whereas the authors attribute the appearance of white folds upon compression to the transfer of particles into the air phase.³⁵ Smaller hydrophilic silica nanoparticles (40–200 nm) have been investigated by Tolani and co-workers at the air/water interface, and only irreversible particle ejection from the interface is reported as the collapse mechanism.²⁵ Upon hydrophobic surface modification, buckling of the fumed silica nanoparticles (200 nm) is observed at air/water⁹ and oil/water interfaces.²⁴ For polystyrene particles, Aveyard et al. have investigated particle sizes ranging from 0.2 to 2.6 μm at air/water and oil/water interfaces. The only collapse mechanism displayed by all the monolayers studied is buckling.^{26,36} Furthermore, monolayers of polystyrene particles placed at the interface between aqueous surfactant solutions and octane have been examined under compression. Since buckling is

INTRODUCTION

Recently, a great deal of attention has been focused on colloidal particles at interfaces owing to their wide range of applications in which the substantial desorption energy of particles is harnessed.¹ One such application is the stabilization of emulsions and foams by decorating the involved fluid interfaces with colloidal particles.^{2–4} The resulting Pickering emulsions and foams⁵ have a plethora of technological utilizations in the cosmetics, pharmaceutical, and food industry.⁶ It is believed that the enhanced stability of Pickering emulsions and foams stems from the formation of an aggregated particulate layer that arrests the coalescence of droplets and bubbles.^{3,7} Thus, the mechanical properties of such particle-laden interfaces play a crucial role in achieving stability.⁸ Furthermore, in many of the aforementioned applications, the interface undergoes large deformations that produce compression and shear stresses; hence, an effective stabilization heavily depends on the flow behavior of the colloidal monolayers.^{7,9,10} In fact, numerous studies have been conducted to link the rheological response of particle-laden interfaces to stability of emulsions and foams.^{11–13} Therefore, it is imperative to advance our understanding of how the mechanical properties of an interface, i.e., the dilatational/shear surface elasticity, are altered by attachment of particles. For example, the method chosen for preparing an interfacial layer, i.e., successive depositions vs subsequent compressions, has been shown to impact the ensuing rheology.^{14,15} Additionally, physical or chemical tuning of the particle wettability by adsorption of ionic surfactants or grafting alkyl chains to the particle surface has been found to be

Received: May 5, 2015

Revised: June 21, 2015

Published: June 22, 2015



observed for all surfactant concentrations studied, the authors argue that folding might be a general mechanism for collapse of particle arrays.²⁸

In all the above-mentioned studies, the uniaxial compression of the interface has been carried out using a Langmuir trough. However, interfacial compression can also be applied by uniform contraction of a particle-laden pendant/sessile drop. Using a particle-laden pendant drop, Ravera et al. have investigated the compressional behavior of a hexane droplet in a dispersion of silica nanoparticles (15 nm) and a cationic surfactant. They report that beyond a critical surfactant concentration buckling occurs upon droplet contraction. The lack of buckling below this concentration is ascribed to the reversible binding of nanoparticles to the interface due to their low hydrophobicity.¹² Asekomhe et al. have studied the contraction of droplets covered by silica particles (13 μm) of two wettabilities and observed particle expulsion or crumpling depending on the particle surface wettability.²² Xu et al. have investigated the behavior of polystyrene particles (3.1 μm) on a sessile water drop in oil medium and have shown that buckling occurs upon droplet contraction.²⁹

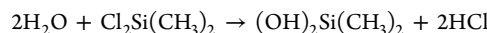
Despite the large body of work on particles at interfaces, the key factors governing the mode of collapse have not been clearly identified. Whereas Aveyard and co-workers have proposed that buckling might be a general collapse mechanism for colloidal arrays,²⁸ Brownian dynamics simulations carried out by Pugnaloni et al. suggest that the collapse mechanism is essentially determined by particle–particle interactions.^{37,38} Moreover, many of the studies mentioned earlier are aimed at determining the particle contact angle using the collapse pressure. This approach is based on the major assumption that the collapse of the monolayer occurs through particle expulsion; therefore, the particle desorption energy can be derived from the obtained collapse pressure.^{35,39–41} In an attempt to connect the earlier studies and to better understand how particle surface properties impact instabilities at fluid interfaces, we have conducted Langmuir trough studies on silica particles with different surface wettabilities at the air/water interface.

The results presented here demonstrate that particle surface wettability impacts the collapse mechanism and its reversibility, illustrating the significance of the strength of colloidal particle binding to a fluid interface and the consequence of interparticle interactions. Furthermore, we show that the presence of an electrolyte in the aqueous subphase plays a crucial role in the effective binding of particles to the interface, structure of the interfacial layer, and the collapse mechanism observed. Our results complement the previous studies and can be exploited in the engineering of interfaces with a preferred collapse mode and a desired stability.

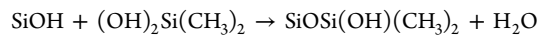
MATERIALS AND METHODS

Surface Modification of Silica Particles. Silica particles used in this study have a nominal size of 1 μm and are purchased from Fiber Optic Center, Inc. Owing to their surface silanol groups, unmodified silica particles are hydrophilic in nature.⁴² To tune the affinity of particles for the fluid interface, deactivation of surface silanol groups is carried out through silanization⁴³ in which dichlorodimethylsilane (DCDMS, 99+, Acros Organics) is chosen as the silanization agent.⁴⁴ During this two-step reaction, alkylsilanols formed by the hydrolysis of DCDMS undergo condensation with silanol groups on the particle surface:⁴⁵

hydrolysis step:



condensation step:



The hydrophobicity of the particle surface thus depends, among other factors,⁴⁶ on the concentration of the silanization agent in the reaction medium. To achieve a range of hydrophobicities, solutions with varying concentration of 10^{-x} M of DCDMS in cyclohexane (extra dry, 99.5%, Acros Organics) are prepared where $x = 1, 2, 3$, and 4. Hereafter, the resulting modified particles are referred to as Sx based on their surface modification, whereas Soo refers to unmodified silica particles. Briefly, for each surface modification, 1 g of silica particles is oven-dried at 60 °C overnight and then mixed with 10 mL of 10^{-x} M DCDMS in extra dry cyclohexane solution. After 30 min sonication, particles are separated via centrifugation (2 min at 4000 rpm) and redispersed in fresh cyclohexane followed by 15 min sonication. Successive centrifugation–redisposition steps are performed twice with chloroform (HPLC grade, Fisher Scientific) and twice with anhydrous ethanol (histological grade, Fisher Scientific), respectively. Silanized particles are isolated and vacuum-dried at 60 °C for 24 h. Extra dry solvents are used in the silanization process because in the presence of water molecules, silanes can aggregate during deposition and may result in a heterogeneous surface morphology.⁴⁷ All glassware is thoroughly cleaned using a sulfuric acid (Certified ACS Plus, Fisher Scientific) and NOCHROMIX (Godax Laboratories, Inc.) mixture followed by rinsing with copious amounts of ultrapure water and vacuum drying. Water used throughout the study has a resistivity of 18.2 MΩ·cm and is obtained from an Advantage A10 Milli-Q System (EMD Millipore, Billerica, MA).

Contact Angle Measurements. To evaluate the extent of silanization, pieces of acid-cleaned silicon wafer are treated with solutions of DCDMS in cyclohexane in a procedure analogous to the one used for modifying the particle surface. Then a droplet of water is placed on the surface of the silanized wafers. The contact angle of the water droplet on the silicon wafer is extracted from the droplet shape using the edge detection feature of a tensiometer (Attention Theta tensiometer, Biolin Scientific, Finland). Contact angle measurements carried out on freshly modified wafers are repeated on the same wafers after being exposed to air for 6 months and to water for 15 h. No substantial contact angle hysteresis is observed in data taken before and after exposure to either air or water, indicating that the surface modification is stable over the time period of each Langmuir trough experiment. The contact angles reported here are averages of all contact angle measurements for a specific silanization (Supporting Information).

In a complementary set of experiments, close-packed monolayers of unmodified and surface-modified silica particles are transferred to a silicon wafer substrate from a Langmuir film at the air/water interface using Langmuir–Schaefer deposition and wetting of a water droplet on these monolayers is assessed in the same fashion. To check for the stability of the particle surface modification, the contact angle of water droplets is again measured on the very same particle monolayers after exposure to air for 6 months. The data before and after exposure to air are in good agreement (Supporting Information), indicating the stability of particle surface modification in air.

Langmuir Trough Measurements. The NIMA Langmuir trough used in this work has dimensions of 14.7 cm by 7 cm with a working area of $A = 78 \text{ cm}^2$. The value of surface pressure (Π), defined as the difference between the surface tension of the bare air/water interface (γ_0) and the effective surface tension of the particle-laden interface (γ), is measured via a Wilhelmy plate hanging from a pressure sensor that is oriented parallel to the major axis of the barriers. Before each experiment, the trough is cleaned with chloroform and then filled with 65 mL of water or aqueous 1.95 M NaCl (extra pure, Acros Organics, Fisher Scientific) solution. To ensure the absence of any surface active impurities, the interface is swept by closing the barriers to $A = 20 \text{ cm}^2$ and is aspirated several times until the surface pressure in this closed-

barrier state is measured to be less than 0.2–0.3 mN/m. To prepare an interfacial film from each sample, 7.5 mg of unmodified/modified silica particles is dispersed in 200 μL of a 70:30 wt % isopropyl alcohol (Certified ACS Plus, Fisher Scientific) and water mixture and sonicated for 2 min. The particle dispersion is deposited on the air/water interface by forming a droplet at the tip of a 100 μL Hamilton syringe and bringing that droplet in contact with the interface at which spreading is driven by Marangoni flow. After careful drop-by-drop deposition of the solution, a waiting time of 20 min is allowed for evaporation of the spreading solvent. Next, compression is carried out by reducing the trough area at 5 cm^2/min , which corresponds to a linear speed of 0.71 cm/min. To check for dynamic effects, measurements at a lower compression speed (0.05 cm/min) are carried out, but no difference in the behavior of the particle layers is observed. To relate the surface pressure isotherms with the microstructure of the interfacial layers, an Olympus BH-3 optical microscope with a charge-coupled-device (CCD) camera is used to image the interfacial films during the compression–expansion cycle. The micrographs presented here are taken using a 10 \times objective and higher magnification snapshots are captured with a 50 \times objective. Isotherm hysteresis is investigated by performing up to 15 consecutive compression–expansion cycles where compression is immediately followed by expansion of the monolayer. Impact of particle wettability on strength and compressibility of the monolayers is evaluated via the static compression modulus (E_0):^{48,49}

$$E_0 = -A \left(\frac{\partial \Pi}{\partial A} \right)_T = - \left(\frac{\partial \Pi}{\partial \ln A} \right)_T \quad (1)$$

which captures the variations in interfacial tension resulting from changes in the interfacial area. All experiments are carried out at room temperature.

RESULTS AND DISCUSSION

Impact of Silanization on Surface Wettability. The effectiveness of the silanization procedure in tuning the surface wettability of silica particles is verified by two types of macroscopic contact angle measurements; Figure 1a displays

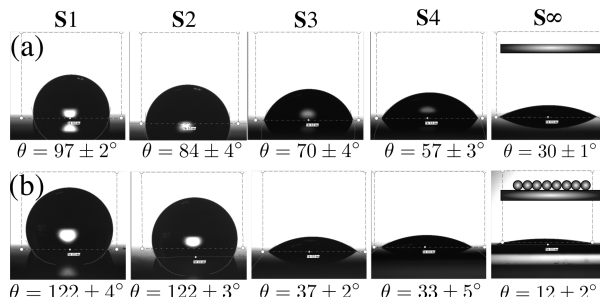


Figure 1. (a) Macroscopic contact angle measurements of a water droplet on unmodified and silanized silicon wafers (surface hydrophobicity increases from right to left). (b) Wetting behavior of a water droplet on close-packed monolayers of unmodified and silanized silica particles (wetting increases from left to right); insets in column S ∞ illustrate the schematic of the sample geometry for each type of measurement.

the contact angle of a water droplet on silicon wafers that have been modified via the same silanization procedure used for the silica particles, and Figure 1b illustrates the wetting behavior of a water droplet on close-packed monolayers of the unmodified and surface-modified silica particles. As can be seen in Figure 1a, by increasing the concentration of the silanization agent, an ascending trend is observed for the measured contact angle. The increase in the contact angle of the water droplet stems from the stronger hydrophobicity of the silicon wafer surface.

More specifically, the surface treatment enables us to turn the hydrophilic surface of the unmodified silicon wafer ($\theta = 30 \pm 1^\circ$) into a hydrophobic surface ($\theta = 97 \pm 2^\circ$) using the S1 protocol, with access to intermediate wettabilities for the S2, S3, and S4 particle surfaces. As shown in Figure 1b, a bimodal wetting behavior is observed when the close-packed monolayers of silica particles are used. The water droplet beaded on S1 and S2 monolayers with contact angles of $\theta = 122 \pm 4^\circ$ and $\theta = 122 \pm 3^\circ$, which in fact points to the hydrophobic nature of these particles. In contrast, spreading of the water droplet with contact angles of $\theta = 37 \pm 2^\circ$ and $\theta = 33 \pm 5^\circ$ is observed for S3 and S4 monolayers, suggesting a more hydrophilic wetting for these particles. The bimodal wetting behavior observed can be interpreted as a transition from a heterogeneous wetting (Cassie–Baxter regime) to a homogeneous wetting (Wenzel regime).⁵⁰ The water droplet spread on a close-packed monolayer of unmodified particles with a very low contact angle ($\theta = 12 \pm 2^\circ$).

Impact of Particle Hydrophobicity on Pressure Isotherms.

We have used the surface pressure (Π)–area (A) isotherms to quantify the impact of surface wettability on the response of the interfacial layers to compressional deformation. The effective surface pressure of particle-laden interfaces results from the configurational entropy of particles and interparticle interactions.^{31,51} The pressure isotherms obtained for all particle monolayers (unmodified silica and S1–S4 silica particles) on a water subphase during the first compression are shown in Figure 2. Distinct features observed in the isotherms are associated with unique morphological transitions. To relate these features to the corresponding phase changes, microscopy images of the most (S1) and least (S4) hydrophobic layers are provided in Figure 3. From these optical images some qualitative information on the interfacial contact angle of the particles can be inferred. As can be seen in Figures 3a–I and 3b–I, the S1 and S4 particles appear optically different upon deposition at the interface although the imaging is carried out with the same microscope settings. Since a larger refractive index mismatch exists between air and silica compared to water and silica, the darker appearance of the S1 (and S2, not shown here) particles is an optical consequence of their larger protrusion into the air phase in comparison with the S4 (and S3, not shown here) particles, which is in good agreement with the macroscopic contact angle measurements ($\theta_{\text{S1}} = 97 \pm 2^\circ$ and $\theta_{\text{S4}} = 57 \pm 3^\circ$).

Despite spreading the same dispersion volume at the interface for all samples, the surface concentration of the trapped particles strongly depends on the particle surface wettability. As illustrated in Figure 2a, the surface pressure remains zero for unmodified silica particles even at the fully compressed state ($A = 20 \text{ cm}^2$), indicating that these particles are not trapped at the interface and fall through the interface upon spreading. This lack of particle surface binding is attributed to dissociation of surface silanol groups, which renders the particle surface negatively charged and highly hydrophilic. Additionally, the air/water interface is believed to carry some negative charge,⁵² and the repulsion between the particle surface and the charged interface further hinders particle binding. In contrast, interfacial entrapment of all hydrophobically modified particles is evident from their pronounced pressure response to changes in trough area.

Three distinct regions can be recognized in each pressure isotherm. Region A denotes the part of the isotherm where the surface pressure is relatively low since well-separated islands of

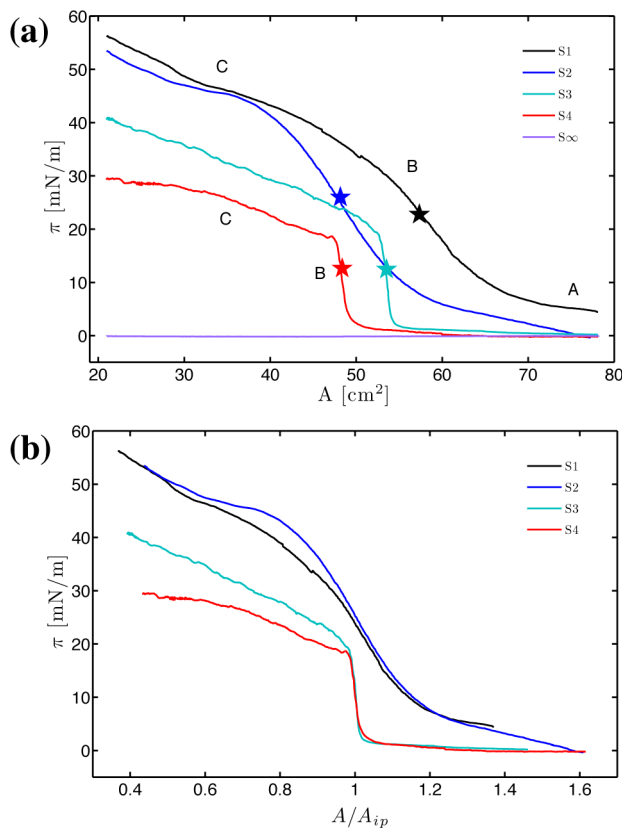


Figure 2. (a) Surface pressure as a function of trough area for unmodified and surface modified silica particles; for each isotherm, the ★ symbol marks the trough area at which a HP structure (A_{ip}) is obtained. (b) Isotherms normalized with trough area at HP order (A_{ip}). Regions A–C correspond to different phases obtained over the course of the compression (see text for more detail).

particles are distributed over the trough, and the interfacial layer contains particle rafts that are separated by particle-void air/water domains. The proximity of particles and the size of clusters appearing in region A strongly depend on the particle surface wettability and resulting particle–particle interactions. In region B, a contiguous network of particles is formed through densification of surface structures, which eventually leads to hexagonal packing (HP) of the particles. The inflection

point of the isotherm in this region (A_{ip}) corresponds to the HP structure²⁴ as verified by optical microscopy. Emergence of meandering striation patterns upon further compression beyond the HP arrangement indicates the onset of deformations out of the interface plane.²⁴ Next, in region C, an abrupt change in the isotherm slope hints at the collapse of the monolayer. The kink observed in the surface pressure isotherm is the hallmark of monolayer collapse.

Although all surface modified particles exhibit interfacial activity, the degree of binding enhancement and the response of each particle type to compression are a strong function of the particle affinity for the interface, which is determined by the surface modification. As can be seen in Figure 2a, the onset of pressure escalation occurs at higher trough areas for S1 and S2 particles and is shifted to lower trough areas for S3 and S4 particles, indicating a better entrapment of the more hydrophobic particle type. Normalizing the pressure isotherm for each sample with respect to the trough area at which the HP structure is obtained (A_{ip}) enables a comparison between particles with different surface modifications. As apparent from Figure 2b, the pressure isotherms for S1 and S3 particles exhibit analogous features to the S2 and S4 isotherms, respectively. This similarity is in accordance with the observed bimodal wetting behavior of the water droplet on silica particle monolayers shown in Figure 1b. Furthermore, the shape of the isotherms is distinct for the two groups (S1 and S2 versus S3 and S4). The rise in pressure occurs softly and gradually for S1 and S2 particles, whereas a sharp and prompt pressure increase is detected for S3 and S4 particles. From this observation, some qualitative information on the nature and strength of particle–particle interactions can be deduced. In essence, a larger number of unmodified silanol groups present on the surface of the S3 and S4 particles results in repulsive electrostatic interactions between the particles. Therefore, by deactivating more and more silanol groups via silanization (shifting toward S1 and S2 samples), the double-layer repulsion is weakened. Additionally, the attractive capillary forces that arise from the distortion of the interface are more appreciable for hydrophobic particles and negligible for hydrophilic particles.⁵³ This phenomenon has been ascribed to methyl groups that render the particle surface chemically heterogeneous.⁹ These assumptions are readily confirmed by inspection of the microscopy images in Figure 3I where upon particle

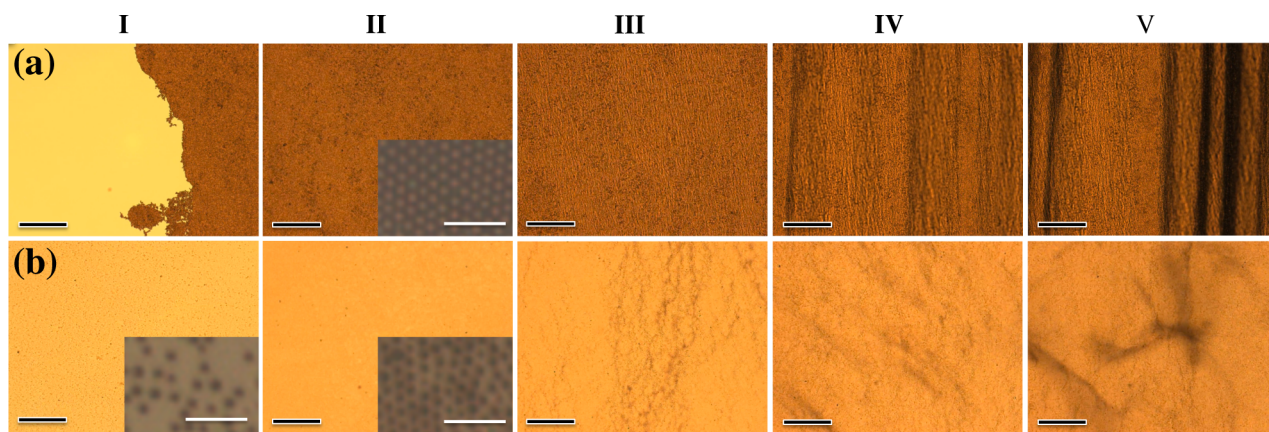


Figure 3. Optical micrographs of (a) S1 and (b) S4 silica particles at the air/water interface captured at different stages of compression: (I) after deposition (inset shows higher magnification; scale bar is 5 μm), (II) HP structure (inset shows higher magnification; scale bar is 5 μm), (III) onset of deformations out of the interface plane, (IV) monolayer collapse, and (V) further compression after collapse. Scale bar is 200 μm .

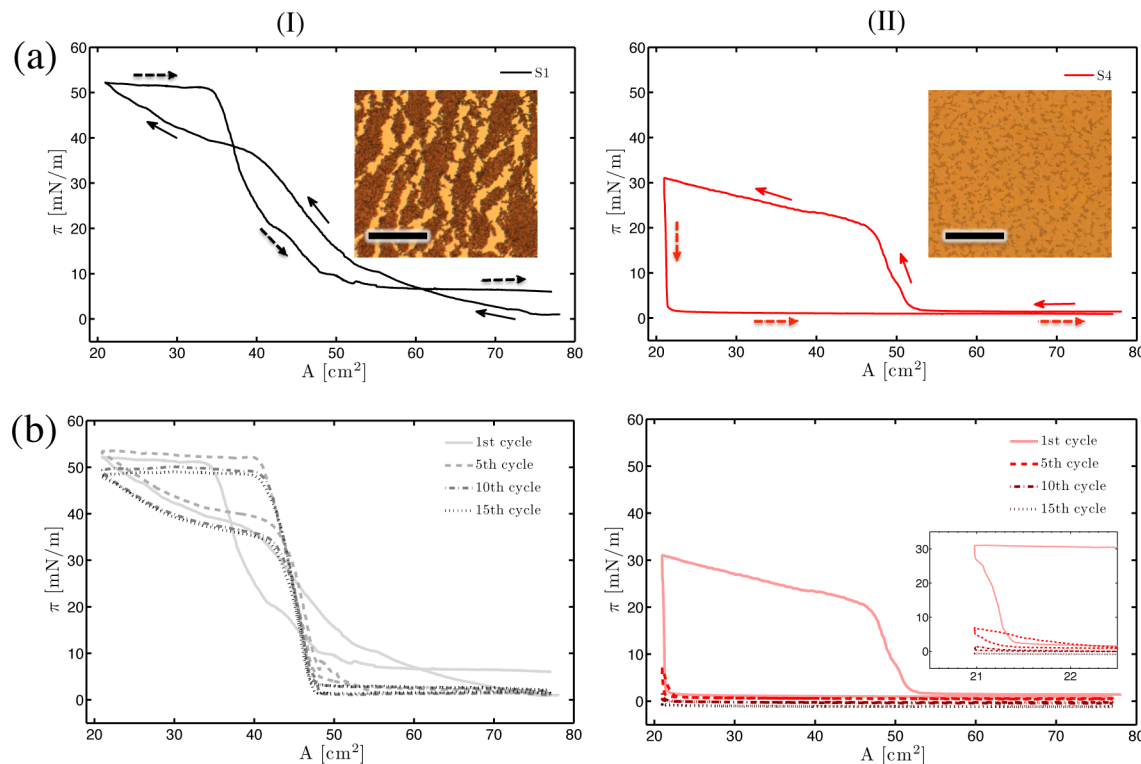


Figure 4. Full compression-expansion isotherms for (I) S1, and (II) S4 particles. In (a) only the first cycle is shown, whereas in (b) the 1st, 5th, 10th, and 15th cycles are depicted. In (a), the solid arrows correspond to compression, and the dashed arrows trace the expansion. The insets in (a) present optical images of the monolayer upon full expansion; scale bars are 100 μ m, and the inset in (b-II) is a zoom-in of the isotherm in the compressed region.

deposition large domains and dense aggregates are captured for S1 (and S2, not shown), in contrast to single particles and smaller clusters observed for S4 (and S3, not shown). The dark region captured in Figure 3a-I is the edge of a particle domain.

Depending on the surface wettability, two collapse mechanisms are observed in region (C). For the more hydrophobic S1 and S2 particles, the formation of a cohesive layer at A_{ip} points to the presence of attractive interparticle interactions. Up to this point, the monolayer resides in a two-dimensional plane (see Figure 3a-II); however, further compression of the film beyond the surface pressures associated with the HP structure induces out-of-plane deformations (see Figure 3a-III). Owing to the attractive nature of particle-particle interactions for S1 and S2, the monolayer behaves as an elastic sheet that buckles. During this process, periodic wrinkles that are oriented parallel to the barriers emerge in three dimensions (see Figure 3a-IV). Further compression of the layer increases the amplitude of the wrinkles, and eventually the applied stress is relaxed via local fold formation. These folds are a few micron wide particle layers that are directed into the subphase with amplitudes deeper than the preceding wrinkles (see Figure 3a-V). In contrast to the solid-like S1 and S2 elastic films, monolayers of the less hydrophobic S3 and S4 particles possess a fluid-like nature and collapse through particle expulsion to the subphase. At the inflection point (A_{ip}), which corresponds to the HP structure, the low contact angle particles are proposed to be in a flocculated state occupying a secondary energy minimum in their pair-potential energy field (Figure 3b-II). This state has been attributed to capillary attractions and dipole-dipole interactions.²⁵ Hence, further lateral compression beyond this point pushes the particles out of this minimum and results in an increased particle-particle

repulsion. Therefore, particles in the weakly cohesive S3 and S4 monolayers are forced to the subphase as the interparticle repulsion surpasses the binding energy of the particle to the interface (Figures 3b-III to 3b-V).⁵⁴ It is worth noting that for all samples the pressure keeps rising even after the monolayer has collapsed. This phenomenon has been attributed to the inhomogeneity of the interfacial layer along the length of the trough, which results in particles having different potential energies.²³

Surface Wettability and Hysteresis. As exhibited in Figure 2b and discussed in the previous section, isotherms and microscopy images of S2 and S3 particles share analogous features with the ones for the S1 and S4 particles. Hence, in this section, we only discuss the findings for the latter two cases in more detail. To investigate the hysteresis phenomenon, surface pressure isotherms of the first compression-expansion cycle are shown in Figure 4a. Additionally, the evolution of hysteresis is examined by successive compression-expansion cycles, and the resulting isotherms are depicted in Figure 4b. Both particle types display considerable hysteresis; nevertheless, the mechanisms leading to the observed hystereses differ considerably and can be traced back to the particle surface wettability.

As can be seen in Figure 4a-I, the area of the hysteresis loop recorded for the S1 (and S2, not shown here) sample is negative. As mentioned in the previous section, these are samples for which collapse of the monolayer occurs through buckling. Further compression of these layers beyond the wrinkled state leads to the formation of folds that are deeply extended into the subphase. These folds do not detach from the interface over the course of compression; hence, folding of S1 and S2 layers is a reversible process. Folds release material back to the interfacial layer upon expansion. During the unfolding

process, the surface area per particle remains constant, and therefore the surface pressure remains constant. Consequently, the surface pressure isotherm exhibits a plateau until all folds open and the monolayer recovers its two-dimensional structure. Expansion beyond this point results in a rapid surface pressure reduction. It should be noted that the surface pressure does not return back to zero, implying that the monolayer has stored a portion of the energy applied during compression. A similar behavior has been reported for monolayers of silica nanoparticles where the particle surface wettability is tuned by adding surfactant.¹⁸ The nonzero pressure of the monolayer at the fully expanded state can be explained by the contiguous structure of the monolayer that is retained through attractive interparticle interactions. We observe with the naked eye that during expansion the interfacial layer detaches from the barriers, whereas particles tend to stay together in a uniform layer and maintain a connected network that encompasses the Wilhelmy plate. Thus, the interfacial network holds up some surface pressure since it does not expand into disconnected aggregates and open structures.⁴ Occasionally, a crack is observed along the Wilhelmy plate and in such a case the surface pressure returns to zero. Whereas the observed hysteresis for monolayers with more hydrophobic character (**S1** and **S2**) stems from wrinkle and fold formation, hysteresis in less hydrophobic samples (**S3** and **S4**) occurs due to expulsion of particles from the interfacial monolayer into the subphase, which is an irreversible collapse mechanism.

The impact of surface modification on interparticle interactions manifests itself in structures that are formed upon full expansion as shown in the insets of Figure 4a. For **S1** and **S2** samples, we observe connected particle rafts, which indicates that strong interparticle attractions hold the particles in contact. Thus, after expansion to the open-barrier state, particles remain part of large clusters and free particle redistribution at the interface is largely arrested. In contrast, for **S3** and **S4** samples, the presence of distinct small-sized clusters points to electrostatic double-layer repulsion that prevents irreversible aggregate formation and clustering. Emergence of segregated domains upon expansion illustrates the weakly cohesive nature of the monolayers.

Since the hysteresis phenomena are dissimilar in the two cases, successive compressions of interfacial layers evolve each system toward a different final state. Pressure isotherms obtained from successive cycles are shown in Figure 4b. Owing to monolayer densification, a horizontal shift in area associated with the pressure lift-off is observed in the first five cycles for the more hydrophobic **S1** and **S2** particles. Moreover, isotherms with a steeper slope are achieved in later cycles since repeated compressions enhance the homogeneity of the monolayer. Part of the initial hysteresis originates from viscous deformations through particle rearrangements at the interface and diminishes after 10 consecutive cycles. Accordingly, deformations in the following cycles are purely elastic accompanied by fully reversible wrinkle and fold formation. In other words, the monolayer is maintained from cycle to cycle through reversible collapse. Analogous to **S1** and **S2** particles, after the first cycle, the onset of the pressure rise for **S3** and **S4** particles is shifted to smaller trough areas in successive cycles. However, the reason behind this shift is the particle loss to the subphase that occurs upon collapse of the monolayer during the first cycle. In contrast to **S1** and **S2** particles, repeated compressions lower the maximum surface pressure attainable for **S3** and **S4** particles in the closed-barrier state, owing to

particle expulsion from the interface that takes place during each and every compression. The continuous particle loss results in a reduced particle surface density and thus a reduced surface pressure.

It is noteworthy that the folding phenomenon observed for more hydrophobic **S1** and **S2** monolayers takes place in the vicinity of the barriers because the surface pressure closer to the barriers is higher than at the center of the trough. The existence of a surface pressure gradient has been validated for hydrophobic silica nanoparticles by measuring the surface pressure at two locations on the trough simultaneously⁵⁵ and is stated to reduce by decreasing the distance between barriers.⁵⁶ The gradient has been attributed to the cohesiveness of hydrophobic monolayers and their high surface viscosity that hinders the immediate propagation of the pressure applied at the barriers.^{55,56} Owing to the presence of the surface pressure gradient along the trough, the collapse pressure is strongly dependent on the number of particles spread at the interface. As illustrated in Figure 5 for **S2** particles, the collapse pressure

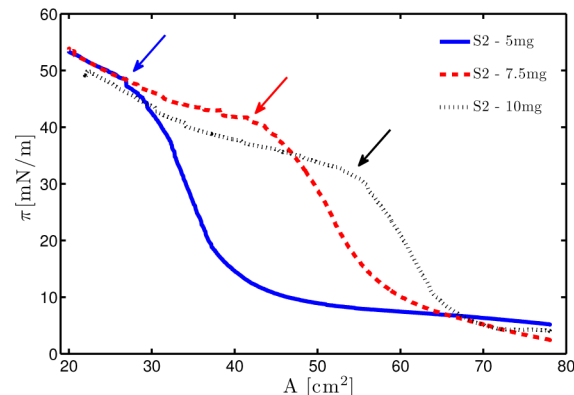


Figure 5. Surface pressure isotherms for **S2** particles with varying initial particle volume. The arrows point to the collapse for each surface concentration.

increases by decreasing the initial surface concentration of particles, which is in agreement with other studies.^{15,25,55,57} This phenomenon is significant for cohesive monolayers formed from more hydrophobic particles and not as pronounced for less hydrophobic samples.^{25,55}

Impact of Electrolyte Addition on Phase Behavior. An important factor that influences the ability of particles to bind to an interface is their surface charge. Dissociation of these surface charges in water followed by spontaneous double-layer formation has been reported to have an impact on the effective particle adsorption to the interface and the contact angle of the particle residing at the interface.⁵⁸ Furthermore, the air/water interface is believed to possess a negative surface potential that stems from hydroxide groups present at the interface and ordering of the water molecules in the vicinity of the interface.^{52,59} Hence, introducing salt to the subphase has profound consequences on the binding capability of charged particles. Moreover, since the particle–particle repulsions are reduced over an electrolyte-rich subphase,^{60,61} the induced collapse mechanism might be different from the one observed for particulate monolayers on water.

Figure 6a illustrates the response of unmodified **S00**, **S1**, and **S4** particle monolayers on an aqueous 1.95 M NaCl subphase in comparison to a water subphase. Isotherms normalized by the area corresponding to the HP structure (A_{hp}) are displayed

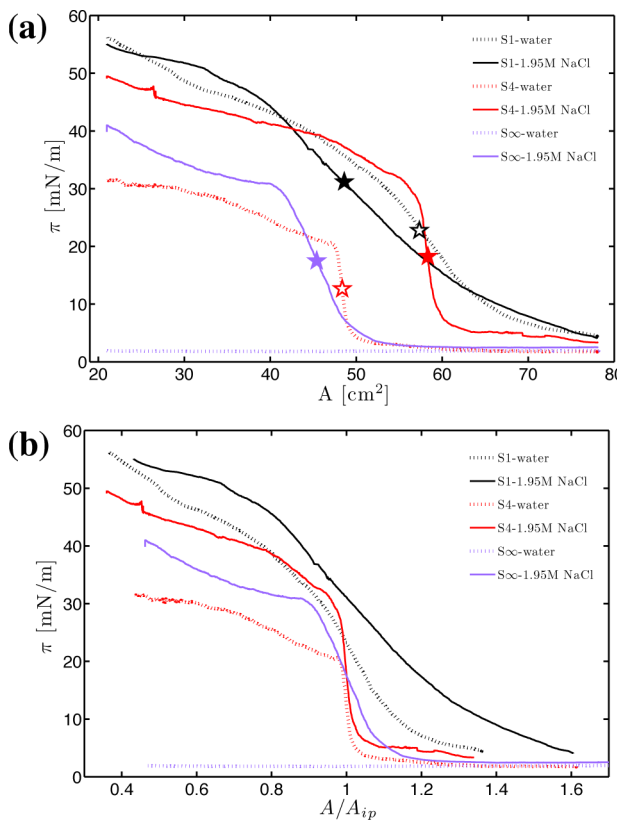


Figure 6. (a) Surface pressure as a function of trough area for unmodified and surface-modified silica particles on water (dashed line) and NaCl aqueous solution (solid line); the open and solid ★ symbols mark the trough area at which a HP structure (A_{ip}) is obtained on water and aqueous 1.95 M NaCl subphase, respectively. (b) Isotherms normalized with trough area at HP structure (A_{ip}).

in Figure 6b. There are a number of features of interest in these isotherms. As shown earlier, the unmodified silica particles, Soo, have a very poor affinity for the air/water interface, and the surface pressure remains essentially zero for all compressions on water (see Figure 2a). Interestingly, the entrapment of unmodified particles is drastically improved on an electrolyte-rich aqueous subphase. This binding enhancement stems from the introduced counterions in the solution that screen the surface charges on the silica particles, shorten the Debye length, and potentially buffer the repulsive interaction between the negative charges on the particle surface and the negatively charged air/water interface.⁶² Analogously, the improvement of S4 particle adsorption on an electrolyte-rich subphase manifests itself in the onset of the pressure rise shifting to a larger trough area. These findings are in accordance with earlier studies that report a change in the contact angle of silica particles upon addition of salt to the subphase.^{63–66} In contrast, the presence of electrolyte does not seem to substantially impact trapping of the more hydrophobic S1 particles, indicating that the majority of surface silanol groups has been deactivated via silanization in good agreement with the contact angle stability (Supporting Information). It is worth mentioning that the buoyancy effects caused by replacing the water subphase ($\rho = 1 \text{ g/cm}^3$) with the aqueous 1.95 M NaCl subphase ($\rho = 1.06 \text{ g/cm}^3$) are negligible since the silica particles have a density of $\rho = 1.8 \text{ g/cm}^3$. The enhanced particle confinement observed over an electrolyte-rich subphase supports the presence of an electrostatic

repulsion between the particle and the air/water interface, which is screened by addition of salt.

Addition of salt affects not only the interaction of charged colloidal particles with the air/water interface but also the particle–particle interactions. This fact can be inferred from microscopy images captured upon deposition of particles on an electrolyte-rich subphase as shown in Figure 7. On a water subphase, only individual particles or clusters with a few particles are observed for the S4 sample (see Figure 3b-I), whereas on an electrolyte-rich subphase particles arrange in extended aggregates composed of a larger number of particles (see Figures 7a-I and 7b-I). Since interparticle interactions—mainly in the case of the unmodified and less hydrophobic particles—are affected by the presence of the electrolyte, addition of salt could also have consequences for the collapse mechanism. In fact, the features observed in the collapse of unmodified and less hydrophobic particles on an electrolyte-rich subphase are brought about by a mechanism different from the two discussed thus far, i.e., particle expulsion to the bulk and wrinkle formation. By compressing the Soo and S4 monolayers on the electrolyte-rich subphase past the HP structure (see Figures 7a-II and 7b-II), particles are forced out of the interface because of their low interfacial position. As can be seen in Figures 7a-III and 7b-III, ejected particles remain connected to the primary interfacial layer by forming additional layers beneath the interface. This point can be further corroborated by comparing the micrographs of S4 particles on the water subphase (Figures 3b-III and 3b-IV) with the ones on the electrolyte-rich subphase (Figures 7b-III and 7b-IV). On the water subphase, the ejected particles have a diffusive appearance as they move away from the focal plane through sedimentation in the water phase. In contrast, on the electrolyte-rich subphase, the ejected particles appear much sharper and in focus as they are arrested beneath the interface upon ejection. This observation points to the presence of attractive interparticle interactions that prevent the expelled particles from escaping into the bulk. As can be seen in the micrographs of the expanded state (see Figures 7a-V and 7b-V), formation of these secondary layers is an irreversible process; hence, successive compressions lead to an increase in their width and thickness. It is noteworthy that not only the collapse mechanism for S4 particles changes on an electrolyte-rich subphase but also the collapse of the monolayer takes place at higher surface pressure values. On the contrary, addition of salt has a negligible impact on the behavior of the S1 particle monolayer under compression and the resulting isotherm, suggesting that the particle–interface and particle–particle interactions are not influenced by addition of salt; therefore, the collapse of the monolayer still happens through wrinkling and folding as depicted in Figure 7c-IV.

From the results obtained for silica monolayers, one can deduce that the presence of electrolytes in the aqueous subphase impacts binding of the charged silica particles studied here and that the collapse mechanism is chiefly determined by the particle–particle interactions and wettability of the particle surface. To validate this hypothesis, we have carried out experiments with monolayers of 1 μm sulfonated polystyrene particles (Invitrogen). In accordance with the unmodified silica particles, an effective trapping can be attained only on an electrolyte-rich subphase because the particles carry a negative surface charge. This particle binding is followed by particle coagulation and formation of large clusters on the aqueous 1.95 M NaCl subphase (see Figure 7d-I). Although the binding

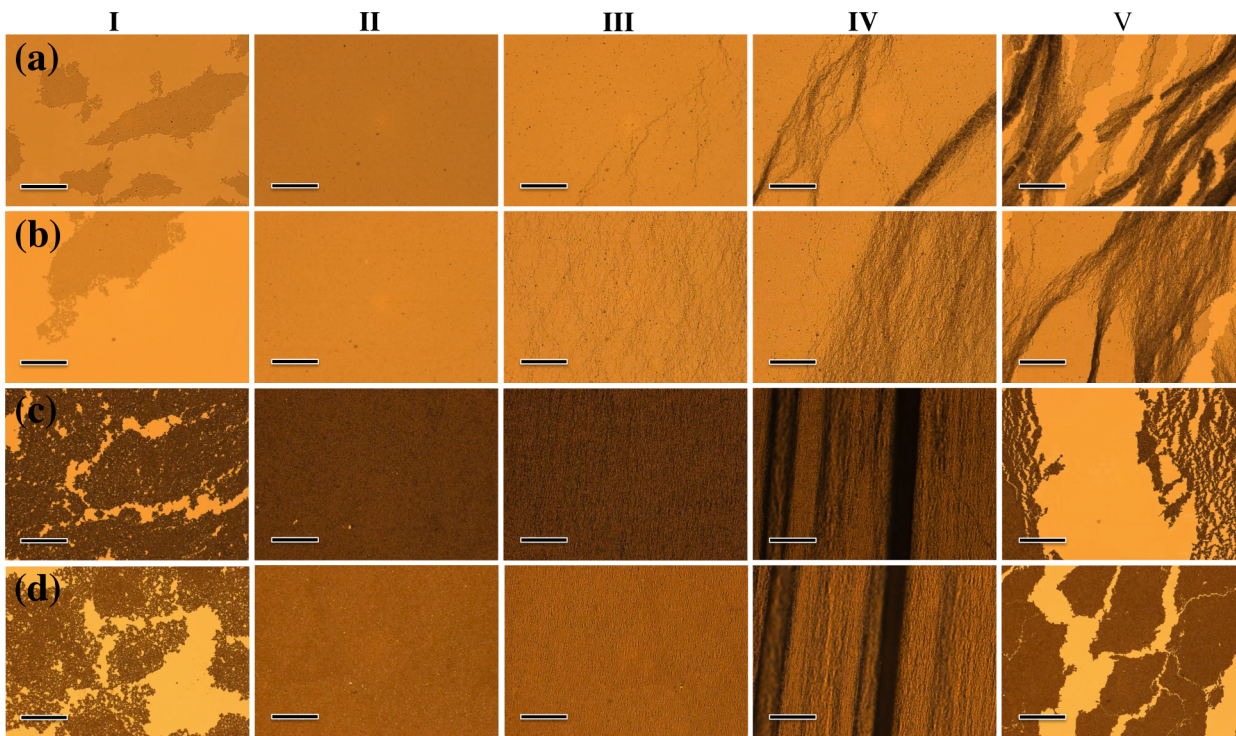


Figure 7. Optical images of (a) unmodified Soo silica, (b) S4 silica, (c) S1 silica, and (d) sulfonated polystyrene particles on an aqueous 1.95 M NaCl subphase captured at different stages of the compression–expansion cycle: (I) after deposition, (II) HP structure, (III) onset of deformations out of the interface plane, (IV) monolayer collapse, and (V) expanded state with fully opened barriers. All scale bars are 200 μ m.

capability of the polystyrene particles resembles that of the unmodified silica particles and the addition of salt improves the interfacial adsorption of particles by screening the particle–interface repulsion in both cases, the response of the polystyrene particle layers to compression and their collapse mechanism are fundamentally different from those of the unmodified inorganic silica layers. Whereas the collapse of the unmodified inorganic silica layers takes place through particle expulsion and multilayer formation, monolayers composed of hydrophobic polymeric polystyrene particles collapse by wrinkling and folding without any particle expulsion to the bulk (see Figure 7d). The enhancement of particle trapping in the presence of electrolyte and the observed collapse mechanism are in agreement with other studies carried out on polystyrene particles.³⁶ In fact, the pressure isotherm and the observed collapse mechanism for polystyrene particles are very similar to the ones obtained for the most hydrophobic S1 particles (see Figures 7c, 7d, and 8). This resemblance in collapse modes stems from the similar surface wettability of the two particles and highlights the crucial role of the particle's hydrophilic/hydrophobic nature in the resulting collapse mechanism. The observed dependence of the collapse mode on the particle surface properties is in excellent agreement with Brownian dynamics simulations by Pugnaloni et al., who studied the effect of interparticle interaction potentials on monolayer collapse upon compression.^{37,38} Briefly, a monolayer of particles interacting via a strong repulsive spherical potential is found to collapse by desorption of the particles to the bulk. However, after employing a short-range attractive potential or a reversible-bond interaction, the applied compression results in stripe-like patterns that desorb from the interface but remain attached to the interfacial monolayer by forming a secondary

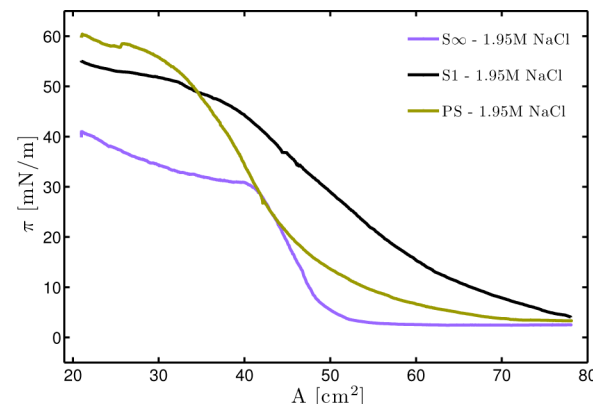


Figure 8. Pressure isotherms for 1 μ m unmodified Soo silica, hydrophobically modified S1 silica, and sulfonated polystyrene particles (PS) on an aqueous 1.95 M NaCl subphase.

layer. Moreover, implementing an elastic irreversible-bond potential leads to collapse of the monolayer through wrinkling.

Static Surface Modulus. Particle surface properties influence the ability of a particle to bind to an interface, the response of an interfacial particulate layer to compression, and the ensuing collapse mechanism. To further quantify the impact of particle surface wettability on the mechanical strength of the particle monolayers, we have assessed the two-dimensional modulus of the monolayers. From the pressure isotherms and microscopy images, it has been established that the surface density of the particles at the inflection point of the isotherm (A_{ip}) is approximately the same for all samples. Therefore, we have evaluated the response of interfacial monolayers in terms of their compressional modulus (E_0) as a function of the applied strain (ϵ), which is defined as:

$$\epsilon = \int_{A_{ip}}^A \frac{dA}{A} = \ln\left(\frac{A}{A_{ip}}\right) \quad (2)$$

As can be seen in Figure 9, plotting the compressional modulus versus the strain provides insight into the strength of the monolayers at different stages of compression. Figure 9a displays the impact of particle wettability on the compressional

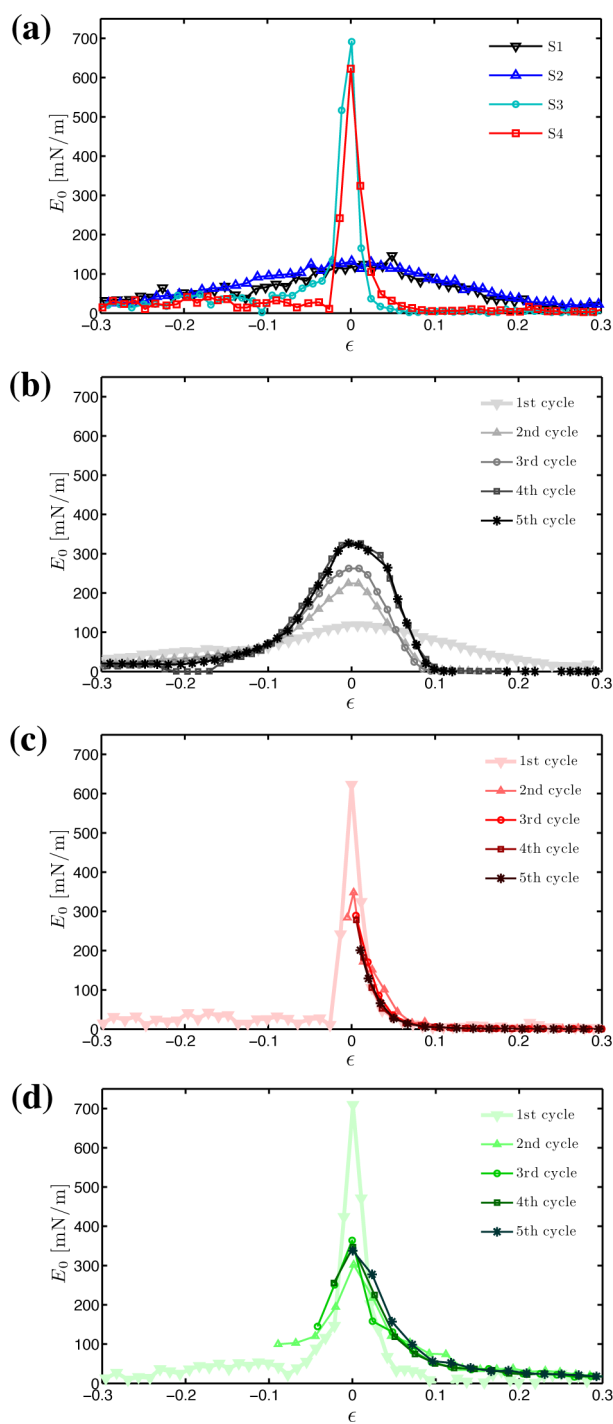


Figure 9. Compressional modulus of interfacial monolayers as a function of strain for (a) silica particles with different wettabilities on water during the first compression; (b) S1 monolayers on water, (c) S4 monolayers on water, and (d) S4 monolayers on an aqueous 1.95 M NaCl subphase during successive compression-expansion cycles.

modulus of the silica monolayers and is derived from the pressure isotherms of Figure 2. The maximum modulus obtained corresponds to the compressional stiffness and mechanical strength of a hexagonally packed monolayer of particles. The soft and gradual increase of the surface pressure observed for the S1 and S2 isotherms in Figure 2 is manifested in a lower compressional modulus of these samples in Figure 9a. In contrast, the less hydrophobic S3 and S4 samples go through a larger maximum owing to their repulsive particle-particle interactions.

Figure 9a reflects on the monolayer modulus during the first cycle for various surface wettabilities; however, successive compressions of a monolayer can alter its response. Depending on the surface properties of the particles, this change in the modulus can stem from particle rearrangements in the monolayer or collapse of the monolayer. Here, we discuss the findings for S1 and S4 monolayers in response to successive compressions. As illustrated in Figure 9b, for the more hydrophobic S1 particles, densification of the surface structure that occurs during the first few cycles gives rise to a stiffer monolayer with a higher modulus. Hence, monolayers composed of more hydrophobic particles exhibit an elastic compressibility after the initial stabilization cycles because their collapse is a fully reversible process. In contrast, by compressing S4 monolayers past the HP structure, particles are forced out of the interface. The irreversible collapse of the monolayer causes the modulus to decline after each compression as shown in Figure 9c. Therefore, the collapse mode plays an influential role in achieving particulate monolayers with a stable compressional modulus.

As discussed in the earlier sections, the presence of electrolyte in the subphase contributes to a better entrapment of the unmodified and less hydrophobic particles and results in the formation of denser aggregates at the interface. Moreover, by switching from a water to an electrolyte-rich subphase, the collapse mechanism for the less hydrophobic S4 monolayers changes (multilayer formation instead of particle expulsion to the bulk). Thus, the impact of salt on the compressibility of the S4 monolayer is embodied in two aspects: the maximum stiffness obtained during the first cycle and the evolution of the monolayer compressibility through successive compressions. By comparing Figures 9c and 9d, it can be seen that during the first compression the S4 monolayer exhibits a higher modulus on an electrolyte-rich subphase and can withstand higher compressions before collapsing. The larger mechanical strength can be ascribed to screening of the double-layer repulsion. Furthermore, replacing water with an electrolyte-rich subphase leads to a divergent impact of successive compressions on the modulus. Whereas on water the interfacial layer presents a lower modulus after each compression, on an electrolyte-rich subphase, the interfacial layer tends to recover through consecutive compressions. As illustrated in Figure 9d, the modulus of the first cycle is the highest and the monolayer exhibits a lower strength on the second cycle. However, the interfacial layer displays some gain in modulus after each following cycle. This can be ascribed to the observed thickening of the interfacial layer by formation of the secondary layers, which results in a higher strength.

CONCLUSIONS

In this work, we have demonstrated that changing the surface wettability of silica particles via silanization affects not only their adsorption to the interface but also the nature and strength of

particle–particle interactions at the interface. The interparticle forces play a key role in the structure of the monolayers formed at the interface and their response to deformation. Consequently, through lateral compression of the monolayers, we observed distinct collapse mechanisms that essentially depend upon the particle surface wettability. Less hydrophobic particles form a fluid-like monolayer that experiences an irreversible collapse through particle expulsion to the bulk. In contrast, the more hydrophobic particles result in a solid-like cohesive monolayer that exhibits a prominent compressional elasticity through reversible wrinkling and folding. In fact, the attractive interparticle interactions arrest the stress relaxation through particle ejection to the subphase. Additionally, pressure isotherms reveal hysteresis for all samples; for less hydrophobic particles, particle loss to the subphase gives rise to the hysteresis, whereas for more hydrophobic monolayers the hysteresis originates from the monolayer densification and viscous deformations through particle rearrangements at the interface. Further, we have illustrated that it is feasible to tune particle–particle and particle–interface interactions by adding electrolytes to the aqueous subphase and found that the addition of salt arrests the particle ejection to the subphase and results in the collapse of the interfacial layers through multilayer formation.

The results presented in this study provide insight into the consequential role of the particle–particle and particle–interface interactions in determining the stability and collapse of particle-laden interfaces. Our findings suggest that the nature of the particle surface can be precisely engineered to control instabilities at a fluid–fluid interface. Additionally, colloidal particles have been reported to experience some long-range repulsive forces at an oil/water interface.^{26,68,69} These forces are believed to act through the oil medium resulting from some hydration water trapped at the particle/oil interface.⁴⁴ Therefore, unique collapse mechanisms might arise by switching from the air/water interface to an oil/water interface.

■ ASSOCIATED CONTENT

S Supporting Information

Microscopy videos showing different collapse mechanisms observed for S1 and S4 monolayers on water and on an electrolyte-rich subphase; contact angle measurements illustrating the long-term stability of the silane modification in air and water; hysteresis phenomenon reflected in the pressure isotherms for the S4 particle monolayers on electrolyte-rich subphase. The Supporting Information is available free of charge on the ACS Publications website at DOI: 10.1021/acs.langmuir.5b01652.

■ AUTHOR INFORMATION

Corresponding Author

*E-mail: kretzschmar@ccny.cuny.edu (I.K.).

Notes

The authors declare no competing financial interest.

■ ACKNOWLEDGMENTS

This work was supported by the National Science Foundation through Awards CBET-1067501 and the MRSEC program at the University of Chicago (DMR-1420709) and the Air Force Office of Scientific Research (AFOSR # FA9550-14-1-0263). S.R. acknowledges partial funding from the NSF PREM program (DMR-0934206); K.D.C. acknowledges partial

support from the NSF (MCB-1413613). B.L. acknowledges the support from ChemMatCARS that is funded by NSF (CHE-1346572). The authors thank Sean Griesemer for his help with the experimental setup.

■ REFERENCES

- (1) Zeng, C.; Bissig, H.; Dinsmore, A. D. Particles on droplets: From fundamental physics to novel materials. *Solid State Commun.* **2006**, *139*, 547–556.
- (2) Simovic, S.; Prestidge, C. A. Nanoparticles of varying hydrophobicity at the emulsion droplet-water interface: Adsorption and coalescence stability. *Langmuir* **2004**, *20*, 8357–8365.
- (3) Blute, I.; Pugh, R. J.; van de Pas, J.; Callaghan, I. Silica nanoparticle sols 1. Surface chemical characterization and evaluation of the foam generation (foamability). *J. Colloid Interface Sci.* **2007**, *313*, 645–655.
- (4) Hunter, T. N.; Wanless, E. J.; Jameson, G. J. Effect of esterically bonded agents on the monolayer structure and foamability of nano-silica. *Colloids Surf., A* **2009**, *334*, 181–190.
- (5) Pickering, S. U. Emulsions. *J. Chem. Soc.* **1907**, *91*, 2001–2021.
- (6) Park, B. J.; Lee, D. Particles at fluid-fluid interfaces: From single-particle behavior to hierarchical assembly of materials. *MRS Bull.* **2014**, *39*, 1089–1096.
- (7) Blute, I.; Pugh, R. J.; van de Pas, J.; Callaghan, I. Silica nanoparticle sols. Part 3: Monitoring the state of agglomeration at the air/water interface using the Langmuir-Blodgett technique. *J. Colloid Interface Sci.* **2009**, *336*, 584–591.
- (8) Monteux, C.; Kirkwood, J.; Xu, H.; Jung, E.; Fuller, G. G. Determining the mechanical response of particle-laden fluid interfaces using surface pressure isotherms and bulk pressure measurements of droplets. *Phys. Chem. Chem. Phys.* **2007**, *9*, 6344–6350.
- (9) Safouane, M.; Langevin, D.; Binks, B. P. Effect of particle hydrophobicity on the properties of silica particle layers at the air-water interface. *Langmuir* **2007**, *23*, 11546–11553.
- (10) Zang, D. Y.; Zhang, Y. J.; Hou, Q. W. Effect of hydrophobicity on tensile rheological properties of silica nanoparticle monolayers at the air-water interface. *Colloids Surf., A* **2012**, *395*, 262–266.
- (11) Stocco, A.; Rio, E.; Binks, B. P.; Langevin, D. Aqueous foams stabilized solely by particles. *Soft Matter* **2011**, *7*, 1260–1267.
- (12) Ravera, F.; Ferrari, M.; Liggieri, L.; Loglio, G.; Santini, E.; Zanobini, A. Liquid-liquid interfacial properties of mixed nanoparticle-surfactant systems. *Colloids Surf., A* **2008**, *323*, 99–108.
- (13) Santini, E.; Ravera, F.; Ferrari, M.; Alfe, M.; Ciajolo, A.; Liggieri, L. Interfacial properties of carbon particulate-laden liquid interfaces and stability of related foams and emulsions. *Colloids Surf., A* **2010**, *365*, 189–198.
- (14) Zang, D. Y.; Rio, E.; Langevin, D.; Wei, B.; Binks, B. P. Viscoelastic properties of silica nanoparticle monolayers at the air-water interface. *Eur. Phys. J. E* **2010**, *31*, 125–134.
- (15) Zang, D. Y.; Rio, E.; Delon, G.; Langevin, D.; Wei, B.; Binks, B. P. Influence of the contact angle of silica nanoparticles at the air-water interface on the mechanical properties of the layers composed of these particles. *Mol. Phys.* **2011**, *109*, 1057–1066.
- (16) Maestro, A.; Guzman, E.; Santini, E.; Ravera, F.; Liggieri, L.; Ortega, F.; Rubio, R. G. Wettability of silica nanoparticle-surfactant nanocomposite interfacial layers. *Soft Matter* **2012**, *8*, 837–843.
- (17) Santini, E.; Kragel, J.; Ravera, F.; Liggieri, L.; Miller, R. Study of the monolayer structure and wettability properties of silica nanoparticles and CTAB using the Langmuir trough technique. *Colloids Surf., A* **2011**, *382*, 186–191.
- (18) Liggieri, L.; Santini, E.; Guzman, E.; Maestro, A.; Ravera, F. Wide-frequency dilatational rheology investigation of mixed silica nanoparticle-CTAB interfacial layers. *Soft Matter* **2011**, *7*, 7699–7709.
- (19) Yazhgur, P. A.; Noskov, B. A.; Liggieri, L.; Lin, S. Y.; Loglio, G.; Miller, R.; Ravera, F. Dynamic properties of mixed nanoparticle/surfactant adsorption layers. *Soft Matter* **2013**, *9*, 3305–3314.
- (20) Lee, Y. L.; Du, Z. C.; Lin, W. X.; Yang, Y. M. Monolayer behavior of silica particles at air/water interface: A comparison

- between chemical and physical modifications of surface. *J. Colloid Interface Sci.* **2006**, *296*, 233–241.
- (21) Ravera, F.; Santini, E.; Loglio, G.; Ferrari, M.; Liggieri, L. Effect of Nanoparticles on the Interfacial Properties of Liquid/Liquid and Liquid/Air Surface Layers. *J. Phys. Chem. B* **2006**, *110*, 19543–19551.
- (22) Asekomhe, S. O.; Chiang, R.; Masliyah, J. H.; Elliott, J. A. W. Some observations on the contraction behavior of a water-in-oil drop with attached solids. *Ind. Eng. Chem. Res.* **2005**, *44*, 1241–1249.
- (23) Bordacs, S.; Agod, A.; Horvolgyi, Z. Compression of Langmuir films composed of fine particles: Collapse mechanism and wettability. *Langmuir* **2006**, *22*, 6944–6950.
- (24) Horozov, T. S.; Binks, B. P.; Aveyard, R.; Clint, J. H. Effect of particle hydrophobicity on the formation and collapse of fumed silica particle monolayers at the oil-water interface. *Colloids Surf., A* **2006**, *282*, 377–386.
- (25) Tolnai, G.; Agod, A.; Kabai-Faix, M.; Kovacs, A. L.; Ramsden, J.; Horvolgyi, Z. Evidence for secondary minimum flocculation of Stober silica nanoparticles at the air-water interface: Film balance investigations and computer simulations. *J. Phys. Chem. B* **2003**, *107*, 11109–11116.
- (26) Aveyard, R.; Clint, J. H.; Nees, D. Small solid particles and liquid lenses at fluid/fluid interfaces. *Colloid Polym. Sci.* **2000**, *278*, 155–163.
- (27) Vella, D.; Aussillous, P.; Mahadevan, L. Elasticity of an interfacial particle raft. *Europhys. Lett.* **2004**, *68*, 212.
- (28) Aveyard, R.; Clint, J. H.; Nees, D.; Quirke, N. Structure and collapse of particle monolayers under lateral pressure at the octane/aqueous surfactant solution interface. *Langmuir* **2000**, *16*, 8820–8828.
- (29) Xu, H.; Melle, S.; Golemanov, K.; Fuller, G. Shape and buckling transitions in solid-stabilized drops. *Langmuir* **2005**, *21*, 10016–10020.
- (30) Monteux, C.; Jung, E.; Fuller, G. G. Mechanical properties and structure of particle coated interfaces: Influence of particle size and bidisperse 2D suspensions. *Langmuir* **2007**, *23*, 3975–3980.
- (31) Garbin, V.; Crocker, J. C.; Stebe, K. J. Forced desorption of nanoparticles from an oil-water interface. *Langmuir* **2012**, *28*, 1663–1667.
- (32) Leahy, B. D.; Pocivavsek, L.; Meron, M.; Lam, K. L.; Salas, D.; Viccaro, P. J.; Lee, K. Y. C.; Lin, B. H. Geometric stability and elastic response of a supported nanoparticle film. *Phys. Rev. Lett.* **2010**, *105*, 4.
- (33) You, S. S.; Rashkov, R.; Kanjanaboons, P.; Calderon, I.; Meron, M.; Jaeger, H. M.; Lin, B. H. Comparison of the mechanical properties of self-assembled langmuir monolayers of nanoparticles and phospholipids. *Langmuir* **2013**, *29*, 11751–11757.
- (34) Schultz, D. G.; Lin, X.-M.; Li, D.; Gebhardt, J.; Meron, M.; Viccaro, P. J.; Lin, B. H. Structure, wrinkling, and reversibility of Langmuir monolayers of gold nanoparticles. *J. Phys. Chem. B* **2006**, *110*, 24522–24529.
- (35) Horvolgyi, Z.; Mate, M.; Daniel, A.; Szalma, J. Wetting behaviour of silanized glass microspheres at water-air interfaces: a Wilhelmy film balance study. *Colloids Surf., A* **1999**, *156*, 501–507.
- (36) Aveyard, R.; Clint, J. H.; Nees, D.; Paunov, V. N. Compression and structure of monolayers of charged latex particles at air/water and octane/water interfaces. *Langmuir* **2000**, *16*, 1969–1979.
- (37) Pugnaloni, L. A.; Ettelaie, R.; Dickinson, E. Computer simulation of the microstructure of a nanoparticle monolayer formed under interfacial compression. *Langmuir* **2004**, *20*, 6096–6099.
- (38) Pugnaloni, L. A.; Ettelaie, R.; Dickinson, E. Brownian dynamics simulation of adsorbed layers of interacting particles subjected to large extensional deformation. *J. Colloid Interface Sci.* **2005**, *287*, 401–414.
- (39) Clint, J. H.; Taylor, S. E. Particle size and interparticle forces of overbased detergents - A Langmuir trough study. *Colloids Surf.* **1992**, *65*, 61–67.
- (40) Tolnai, G.; Csempesz, F.; Kabai-Faix, M.; Kalman, E.; Keresztes, Z.; Kovacs, A. L.; Ramsden, J. J.; Horvolgyi, Z. Preparation and characterization of surface-modified silica-nanoparticles. *Langmuir* **2001**, *17*, 2683–2687.
- (41) Horvolgyi, Z.; Nemeth, S.; Fendler, J. H. Monoparticulate layers of silanized glass spheres at the water-air interface: Particle-particle and particle-subphase interactions. *Langmuir* **1996**, *12*, 997–1004.
- (42) Barthel, H. Surface interactions of dimethylsiloxy group-modified fumed silica. *Colloids Surf., A* **1995**, *101*, 217–226.
- (43) Brandriss, S.; Margel, S. Synthesis and characterization of self-assembled hydrophobic monolayer coatings of silica colloids. *Langmuir* **1993**, *9*, 1232–1240.
- (44) Horozov, T. S.; Aveyard, R.; Clint, J. H.; Binks, B. P. Order-disorder transition in monolayers of modified monodisperse silica particles at the octane-water interface. *Langmuir* **2003**, *19*, 2822–2829.
- (45) Ngai, T., Bon, S., Eds.; *Particle-Stabilized Emulsions and Colloids*; Royal Society of Chemistry: London, 2014; pp 140–144.
- (46) Hansen, P. H. F.; Ršodner, S.; Bergstroš, L. Structural characterization of dense colloidal films using a modified pair distribution function and Delaunay triangulation. *Langmuir* **2001**, *17*, 4867–4875.
- (47) Diebold, R. M.; Clarke, D. R. Smooth, aggregate-free self-assembled monolayer deposition of silane coupling agents on silicon dioxide. *Langmuir* **2012**, *28*, 15513–15520.
- (48) Gopal, A.; Lee, K. Y. C. Headgroup percolation and collapse of condensed Langmuir monolayers. *J. Phys. Chem. B* **2006**, *110*, 22079–22087.
- (49) Mendoza, A. J.; Guzman, E.; Martinez-Pedrero, F.; Ritacco, H.; Rubio, R. G.; Ortega, F.; Starov, V. M.; Miller, R. Particle laden fluid interfaces: Dynamics and interfacial rheology. *Adv. Colloid Interface Sci.* **2014**, *206*, 303–319.
- (50) San-Miguel, A.; Behrens, S. H. Influence of nanoscale particle roughness on the stability of pickering emulsions. *Langmuir* **2012**, *28*, 12038–12043.
- (51) Petkov, P. V.; Danov, K. D.; Kralchevsky, P. A. Surface pressure isotherm for a monolayer of charged colloidal carticles at a water/nonpolar-fluid interface: Experiment and theoretical model. *Langmuir* **2014**, *30*, 2768–2778.
- (52) Beloqui Redondo, A.; Jordan, I.; Ziazadeh, I.; Kleibert, A.; Giorgi, J. B.; Wšrner, H. J.; May, S.; Abbas, Z.; Brown, M. A. Nanoparticle-induced charge redistribution of the air-water interface. *J. Phys. Chem. C* **2015**, *119*, 2661–2668.
- (53) Onoda, G. Y. Direct observation of two-dimensional, dynamic clustering and ordering with colloids. *Phys. Rev. Lett.* **1985**, *55*, 226–229.
- (54) Bordacs, S.; Agod, A.; Horvolgyi, Z. Compression of Langmuir films composed of fine particles: Collapse mechanism and wettability. *Langmuir* **2006**, *22*, 6944–6950.
- (55) Matž, M.; Fendler, J. H.; Ramsden, J. J.; Szalma, J.; Horvolgyi, Z. Eliminating surface pressure gradient effects in contact angle determination of nano- and microparticles using a film balance. *Langmuir* **1998**, *14*, 6501–6504.
- (56) Bykov, A. G.; Noskov, B. A.; Loglio, G.; Lyadinskaya, V. V.; Miller, R. Dilatational surface elasticity of spread monolayers of polystyrene microparticles. *Soft Matter* **2014**, *10*, 6499–6505.
- (57) Cicuta, P.; Vella, D. Granular character of particle rafts. *Phys. Rev. Lett.* **2009**, *102*, 138302.
- (58) Garbin, V.; Crocker, J. C.; Stebe, K. J. Nanoparticles at fluid interfaces: Exploiting capping ligands to control adsorption, stability and dynamics. *J. Colloid Interface Sci.* **2012**, *387*, 1–11.
- (59) Saykally, R. J. Air/water interface: Two sides of the acid-base story. *Nat. Chem.* **2013**, *5*, 82–84.
- (60) Park, B. J.; Pantina, J. P.; Furst, E. M.; Oettel, M.; Reynaert, S.; Vermant, J. Direct measurements of the effects of salt and surfactant on interaction forces between colloidal particles at water-oil interfaces. *Langmuir* **2008**, *24*, 1686–1694.
- (61) Park, B. J.; Furst, E. M. Attractive interactions between colloids at the oil-water interface. *Soft Matter* **2011**, *7*, 7676–7682.
- (62) Horvolgyi, Z.; Nemeth, S.; Fendler, J. H. Spreading of hydrophobic silica beads at water-air interfaces. *Colloids Surf., A* **1993**, *71*, 327–335.
- (63) Kostakis, T.; Ettelaie, R.; Murray, B. S. Effect of high salt concentrations on the stabilization of bubbles by silica particles. *Langmuir* **2006**, *22*, 1273–1280.

- (64) Horozov, T. S.; Binks, B. P.; Gottschalk-Gaudig, T. Effect of electrolyte in silicone oil-in-water emulsions stabilised by fumed silica particles. *Phys. Chem. Chem. Phys.* **2007**, *9*, 6398–6404.
- (65) Wu, W.; Giese, R. F., Jr.; van Oss, C. J. Linkage between ζ -potential and electron donicity of charged polar surfaces 1. Implications for the mechanism of flocculation of particle suspensions with plurivalent counterions. *Colloids Surf, A* **1994**, *89*, 241–252.
- (66) Paunov, V. N.; Binks, B. P.; Ashby, N. P. Adsorption of charged colloid particles to charged liquid surfaces. *Langmuir* **2002**, *18*, 6946–6955.
- (67) Ishida, N.; Kusaka, Y.; Ushijima, H. Hydrophobic attraction between silanated silica surfaces in the absence of bridging bubbles. *Langmuir* **2012**, *28*, 13952–13959.
- (68) Pieranski, P. Two-dimensional interfacial colloidal crystals. *Phys. Rev. Lett.* **1980**, *45*, 569–572.
- (69) Oettel, M.; Dietrich, S. Colloidal interactions at fluid interfaces. *Langmuir* **2008**, *24*, 1425–1441.